AIAA JOURNAL
Vol. 38, No. 5, May 2000

Fracture Mode Separation for Delamination in Platelike Composite Structures

Z. Yang* and C. T. Sun†
Purdue University, West Lafayette, Indiana 47907-1282
and
J. Wang‡
NASA Langley Research Center, Hampton, Virginia 23681-2199

A computationally efficient approach combining a plate crack-tip element model and a mixed-mode separation technique was developed to calculate mode mixities and stress intensity factors for delamination in platelike composite structures. The crack-tip element was based on classical plate theory, assuming the delamination surfaces to be traction free. Fracture mode separation was achieved by equating the total strain energy release rate from classical plate theory with that from the three-dimensional near-tip solution, along with two supplementary finite element analyses for special loadings. Using this approach, the separation of fracture modes under any other load combinations can easily be carried out. Numerical results showed that the present method gives good evaluations of the mixed-mode stress intensity factors.

Introduction

DELAMINATION is a concern in the analysis and design of advanced composite laminated structures. Edge delamination or embedded delamination may occur in multidirectional composite laminates as a result of mechanical, hygrothermal, or combined loadings. Delamination in composite laminates is basically an interfacial crack between two highly anisotropic laminae. Since Williams[1] found in 1959 that the near crack-tip stress field possesses an oscillatory characteristic for a crack between two dissimilar isotropic materials, interfacial crack problems have been investigated by, among others, England,[2] Rice and Sih,[3] Malysev and Salganik,[4] Sun and Jih,[5] Hutchinson et al.,[6] and Rice[7] for isotropic media, and Gotoh,[8] Clements,[9] Willis,[10] Wang and Choi,[11,12] Ting,[13] Bassani and Qu,[14] Sun and Manoharan,[15,16] Wu,[17] Suo,[18] Gao et al.,[19] Hwu,[20,21] and Deng[22] for anisotropic media. The oscillatory behavior of the near-tip stress and displacement fields associated with interfacial cracks and the unusual unit of the stress intensity factors[7] have been the center of attention.

Fracture criteria are usually given in strain energy release rates or stress intensity factors. For mixed mode fracture partitioning the three fracture modes is essential. For interfacial crack problems such as delamination in composite laminates, however, strain energy release rates for individual modes of fracture do not exist because of their oscillatory nature near the crack tip.[5] Finite element analyses have shown that the strain energy release rate components are mesh-dependent, although the total strain energy release rate is well defined. Consequently, the use of strain energy release rates of the individual fracture modes to establish fracture criteria for interfacial cracks is not feasible. As a result, stress intensity factors, whatever forms they may take, are used.

Several methods have been introduced to calculate stress intensity factors for interfacial cracks. Based on the J-integral, Matos et al.[23] proposed a finite element method for calculating the stress intensity factors for an interfacial crack in isotropic media. Sun and Qian[24] employed the relation between the ratio of near-tip crack surface displacements and the ratio of stress intensity factors in conjunction with the calculation of the total strain energy release rate to calculate the stress intensity factors for interfacial cracks between two dissimilar isotropic media. Subsequently, Qian and Sun[25,26] extended the preceding method to interlaminar cracks in composite laminates. These finite element-based methods by Matos et al.[23] and Sun and Qian[24] are generally quite efficient. However, if the crack is in a platelike structure, the K-dominance zone is very small; and very fine meshes are required to obtain accurate results for stress intensity factors. Thus, for platelike structures, computationally more efficient methods are desired.

Schapery and Davidson[27] developed a plate crack-tip element to calculate the stress intensity factors for cracks in homogeneous isotropic solids. The total strain energy release rate was expressed in terms of a crack-tip force and crack-tip moment. The stress intensity factors were decoupled using an additional finite element analysis. The crack-tip element has also been used to predict the stress intensity factors for interfacial cracks in isotropic media[28] and composites.[29–31] Its application was limited either to two-dimensional composites problems with only two fracture modes or to three-dimensional problems with isotropic bimaterials. For multidirectional composite laminates the angle plies had to be smeared into an equivalent orthotropic layer. To avoid the difficulty of determining unknown coefficients in the crack-tip element analysis for general laminates, Refs. 28, 30, and 31 proposed a so-called $\beta = 0$ method (where β is a generalization of one of Dundurs' parameters for isotropic bimaterials) by modifying the material properties of the two layers immediately below and above the crack. The $\beta = 0$ assumption automatically removes the oscillatory nature of the crack-tip stress and displacement fields, but it can also lead to less accurate evaluations of the stress intensity factors as this modification may alter the characteristics of the interfacial crack.

In the present study a computationally efficient approach combining a plate crack-tip element model and a fracture mode separation technique was developed to calculate mode mixities for delamination cracks in composite laminates. Composite laminates with arbitrary fiber orientations were considered. The plate crack-tip element was derived based on classical laminated-plate theory. The applied loads on the element were fully characterized with two crack-tip forces and one crack-tip moment. Fracture mode separation was achieved by comparing the total strain energy release rate from plate theory with that from the three-dimensional near-tip solution, along with two supplementary finite element analyses for special loadings. Stress intensity factors were uniquely related to the crack-tip forces

Presented as Paper 98-2024 at the AIAA/ASME/ASCE/AHS/ASC 39th Structures, Structural Dynamics, and Materials Conference, Long Beach, CA, 20–23 April 1998; received 5 November 1998; revision received 25 August 1999; accepted for publication 30 August 1999.

*Graduate Research Assistant, School of Aeronautics and Astronautics. Student Member AIAA.

†Neil A. Armstrong Professor, School of Aeronautics and Astronautics. Fellow AIAA.

‡Aerospace Engineer, Mail Stop 240, Structures Division. Senior Member AIAA.

and moment. Mode mixities under any other load combinations can thus be calculated analytically. Three numerical examples for delamination in laminates under various loads were presented to illustrate the procedure. The results indicated that the stress intensity factors could be calculated accurately using the present crack-tip element method.

Plate Crack-Tip Element Analysis

Depicted in Fig. 1 is a plate crack-tip element (CTE) with the crack front parallel to the y axis. The dimension of the CTE in the y direction is unity. This element represents a portion of the two-dimensional crack front in a general composite laminate containing a delamination crack. The assumption is made that the crack lies in a plane parallel to the midplane (the x–y plane) of the laminate. The entire crack front in the laminate may be straight or curved; however, the length of the element in the y direction is assumed to be short enough so that the crack front within this element can be assumed straight. The assumption is further made that the lengths of the cracked and uncracked regions comprising the element, a and b, are large compared to the laminate thickness but are sufficiently small so that the in-plane forces and bending moment are uniform within the element. In addition, transverse shear forces and contact and interpenetration between the crack surfaces are assumed to be absent.

Now consider the plate CTE under in-plane axial loads N, N_1, and N_2; in-plane shear loads S, S_1, and S_2; and bending moments M, M_1, and M_2 (Fig. 1). From overall equilibrium of the element, we have

$$N = N_1 + N_2 \tag{1a}$$

$$M = M_1 + M_2 - N_1 t_2/2 + N_2 t_1/2 \tag{1b}$$

$$S = S_1 + S_2 \tag{1c}$$

From equilibrium of the upper arm of the element in Fig. 2, we obtain

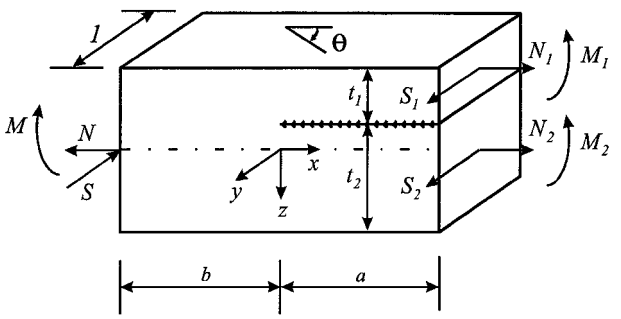

Fig. 1 CTE under in-plane forces and out-of-plane moment.

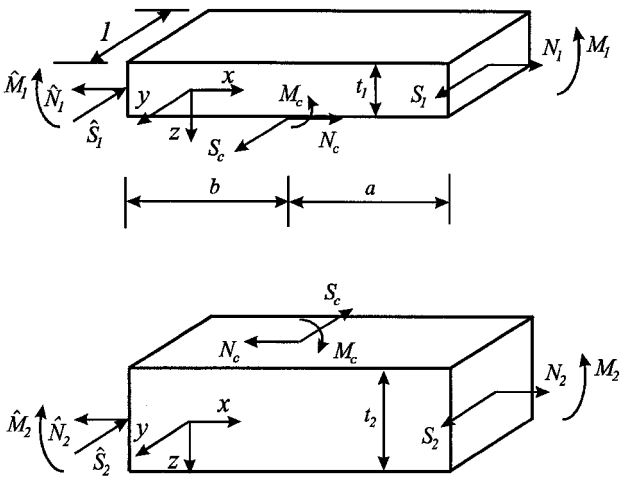

Fig. 2 Free-body diagram for arms bounding crack in the CTE.

$$N_c = \hat{N}_1 - N_1 \tag{2a}$$

$$M_c = \hat{M}_1 - M_1 - N_c t_1/2 \tag{2b}$$

$$S_c = \hat{S}_1 - S_1 \tag{2c}$$

where N_c, M_c, and S_c are the concentrated crack-tip axial force, moment, and shear force, respectively.

Assuming that the crack advances a distance Δa under the crack-tip forces and moment, the total strain energy release rate G can be calculated from the work needed to close the crack increment according to Irwin's virtual crack closure method. We thus have

$$G = (1/2\Delta a)[N_c(\Delta u_1 - \Delta u_2) + M_c(\Delta\varphi_1 - \Delta\varphi_2) + S_c(\Delta v_1 - \Delta v_2)] \tag{3}$$

where $(\Delta u_1 - \Delta u_2)$, $(\Delta v_1 - \Delta v_2)$, and $(\Delta\varphi_1 - \Delta\varphi_2)$ are the relative displacements and rotation of the two arms at the original crack tip, respectively. In Eq. (3) subscripts 1 and 2 denote the upper and lower arms, respectively, and u, v, and φ denote the displacements in the x and y directions and the rotation in the x–z plane, respectively. Only the midplane normal strain ε_x in the x direction, the shear strain γ_{xy} in the x–y plane, and the curvature κ_x in the x direction are nontrivial deformations. Based on classical laminated-plate theory, the equations relating the midplane strains and curvature to the force and moment resultants for the uncracked portion of the element as a whole are given by

$$\begin{Bmatrix} N \\ S \\ M \end{Bmatrix} = \begin{bmatrix} A_{11} & A_{16} & B_{11} \\ A_{16} & A_{66} & B_{16} \\ B_{11} & B_{16} & D_{11} \end{bmatrix} \begin{Bmatrix} \varepsilon_x \\ \gamma_{xy} \\ \kappa_x \end{Bmatrix} \tag{4}$$

or, in their inverted form,

$$\begin{Bmatrix} \varepsilon_x \\ \gamma_{xy} \\ \kappa_x \end{Bmatrix} = \begin{bmatrix} A'_{11} & A'_{16} & B'_{11} \\ A'_{16} & A'_{66} & B'_{16} \\ B'_{11} & B'_{16} & D'_{11} \end{bmatrix} \begin{Bmatrix} N \\ S \\ M \end{Bmatrix} \tag{5}$$

The nine elements in the square matrix in Eq. (4) are the extensional, coupling, and bending stiffnesses of the laminate,[32] respectively. Similarly, for the upper constituent of the uncracked portion (Fig. 2), we have

$$\begin{Bmatrix} \hat{N}_1 \\ \hat{S}_1 \\ \hat{M}_1 \end{Bmatrix} = \begin{bmatrix} \bar{A}_{11} & \bar{A}_{16} & \bar{B}_{11} \\ \bar{A}_{16} & \bar{A}_{66} & \bar{B}_{16} \\ \bar{B}_{11} & \bar{B}_{16} & \bar{D}_{11} \end{bmatrix} \begin{Bmatrix} \hat{\varepsilon}_x^{(1)} \\ \hat{\gamma}_{xy}^{(1)} \\ \hat{\kappa}_x^{(1)} \end{Bmatrix} \tag{6}$$

The deformations given by Eqs. (5) and (6) are related by

$$\begin{Bmatrix} \hat{\varepsilon}_x^{(1)} \\ \hat{\gamma}_{xy}^{(1)} \\ \hat{\kappa}_x^{(1)} \end{Bmatrix} = \begin{Bmatrix} \varepsilon_x - \kappa_x t_2/2 \\ \gamma_{xy} \\ \kappa_x \end{Bmatrix} \tag{7}$$

From Eqs. (5–7) we obtain

$$\begin{Bmatrix} \hat{N}_1 \\ \hat{M}_1 \\ \hat{S}_1 \end{Bmatrix} = \begin{bmatrix} a_{11} & a_{12} & a_{13} \\ a_{21} & a_{22} & a_{23} \\ a_{31} & a_{32} & a_{33} \end{bmatrix} \begin{Bmatrix} N \\ M \\ S \end{Bmatrix} \tag{8}$$

where

$$a_{11} = \bar{A}_{11}A'_{11} + \bar{A}_{16}A'_{16} + B'_{11}(\bar{B}_{11} - \bar{A}_{11}t_2/2)$$

$$a_{12} = \bar{A}_{11}B'_{11} + \bar{A}_{16}B'_{16} + D'_{11}(\bar{B}_{11} - \bar{A}_{11}t_2/2)$$

$$a_{13} = \bar{A}_{11}A'_{16} + \bar{A}_{16}A'_{66} + B'_{16}(\bar{B}_{11} - \bar{A}_{11}t_2/2)$$

$$a_{21} = \bar{B}_{11}A'_{11} + \bar{B}_{16}A'_{16} + B'_{11}(\bar{D}_{11} - \bar{B}_{11}t_2/2)$$

$$a_{22} = \bar{B}_{11}B'_{11} + \bar{B}_{16}B'_{16} + D'_{11}(\bar{D}_{11} - \bar{B}_{11}t_2/2)$$

$$a_{23} = \bar{B}_{11}A'_{16} + \bar{B}_{16}A'_{66} + B'_{16}(\bar{D}_{11} - \bar{B}_{11}t_2/2)$$

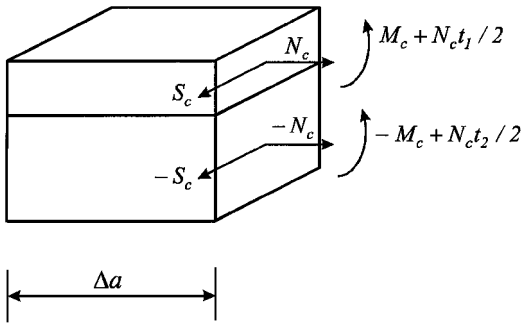

Fig. 3 Statically equivalent loading on arms bounding crack in the CTE.

$$a_{31} = \bar{A}_{16}A'_{11} + \bar{A}_{66}A'_{16} + B'_{11}(\bar{B}_{16} - \bar{A}_{16}t_2/2)$$

$$a_{32} = \bar{A}_{16}B'_{11} + \bar{A}_{66}B'_{16} + D'_{11}(\bar{B}_{16} - \bar{A}_{16}t_2/2)$$

$$a_{33} = \bar{A}_{16}A'_{16} + \bar{A}_{66}A'_{66} + B'_{16}(\bar{B}_{16} - \bar{A}_{16}t_2/2)$$

Equations (2) and (8) show that the loading on the plate CTE is fully characterized by N_c, M_c, and S_c.

Following Schapery and Davidson,[27] we next consider the two arms bounding the crack subjected to the equivalent crack-tip loading N_c, M_c, and S_c (Fig. 3).

The plate constitutive equations for the upper arm are

$$\begin{Bmatrix} \varepsilon_x^{(1)} \\ \gamma_{xy}^{(1)} \\ \kappa_x^{(1)} \end{Bmatrix} = \begin{bmatrix} \bar{A}'_{11} & \bar{A}'_{16} & \bar{B}'_{11} \\ \bar{A}'_{16} & \bar{A}'_{66} & \bar{B}'_{16} \\ \bar{B}'_{11} & \bar{B}'_{16} & \bar{D}'_{11} \end{bmatrix} \begin{Bmatrix} N_c \\ S_c \\ M_c + N_c t_1/2 \end{Bmatrix} \tag{9}$$

where $\varepsilon_x^{(1)}$, $\gamma_{xy}^{(1)}$, and $\kappa_x^{(1)}$ are the midplane deformations of the upper arm. The displacement increments Δu_1 and Δv_1 and rotation increment $\Delta\varphi_1$ of the bottom surface at the crack tip are given by

$$\Delta u_1 = \Delta a\left(\varepsilon_x^{(1)} + \kappa_x^{(1)} t_1 \middle| 2\right) \tag{10a}$$

$$\Delta v_1 = \Delta a \gamma_{xy}^{(1)} \tag{10b}$$

$$\Delta\varphi_1 = \Delta a \kappa_x^{(1)} \tag{10c}$$

Likewise, for the lower arm we have

$$\begin{Bmatrix} \varepsilon_x^{(2)} \\ \gamma_{xy}^{(2)} \\ \kappa_x^{(2)} \end{Bmatrix} = \begin{bmatrix} \bar{\bar{A}}'_{11} & \bar{\bar{A}}'_{16} & \bar{\bar{B}}'_{11} \\ \bar{\bar{A}}'_{16} & \bar{\bar{A}}'_{66} & \bar{\bar{B}}'_{16} \\ \bar{\bar{B}}'_{11} & \bar{\bar{B}}'_{16} & \bar{\bar{D}}'_{11} \end{bmatrix} \begin{Bmatrix} -N_c \\ -S_c \\ -M_c + N_c t_2/2 \end{Bmatrix} \tag{11}$$

The crack openings Δu_2 and Δv_2 and rotation $\Delta\varphi_2$ of the top surface of the lower arm at the crack tip caused by the assumed crack extension Δa are

$$\Delta u_2 = \Delta a\left(\varepsilon_x^{(2)} + \kappa_x^{(2)} t_2 \middle| 2\right) \tag{12a}$$

$$\Delta v_2 = \Delta a \gamma_{xy}^{(2)} \tag{12b}$$

$$\Delta\varphi_2 = \Delta a \kappa_x^{(2)} \tag{12c}$$

Substitution of Eqs. (10) and (12) into Eq. (3) yields

$$G = \tfrac{1}{2}\left(c_{11}N_c^2 + c_{22}M_c^2 + c_{33}S_c^2 + 2c_{12}N_cM_c + 2c_{13}N_cS_c + 2c_{23}M_cS_c\right) \tag{13}$$

where

$$c_{11} = \bar{A}'_{11} + \bar{\bar{A}}'_{11} + \bar{B}'_{11}t_1 - \bar{\bar{B}}'_{11}t_2 + \bar{D}'_{11}t_1^2 \middle| 4 + \bar{\bar{D}}'_{11}t_2^2 \middle| 4$$

$$c_{22} = \bar{D}'_{11} + \bar{\bar{D}}'_{11}, \qquad c_{33} = \bar{A}'_{66} + \bar{\bar{A}}'_{66}$$

$$c_{12} = \bar{B}'_{11} + \bar{\bar{B}}'_{11} + \bar{D}'_{11}t_1/2 - \bar{\bar{D}}'_{11}t_2/2$$

$$c_{13} = \bar{A}'_{16} + \bar{\bar{A}}'_{16} + \bar{B}'_{16}t_1/2 - \bar{\bar{B}}'_{16}t_2/2, \qquad c_{23} = \bar{B}'_{16} + \bar{\bar{B}}'_{16}$$

Note that the preceding six constants, $c_{11}, \ldots, c_{33}$, are independent of loads.

For two-dimensional problems $S_1 = S_2 = S = 0$, and Eq. (13) reduces to

$$G = \tfrac{1}{2}\left(c_{11}N_c^2 + c_{22}M_c^2 + 2c_{12}N_cM_c\right) \tag{14}$$

which is identical to the expression for the total strain energy release rate given in Ref. 27.

Strain Energy Release Rates and Stress Intensity Factors

Beacuse of their oscillatory nature, the strain energy release rates for the three fracture modes do not exist for interfacial cracks. However, for a finite crack extension Δa the virtual crack closure integrals can always be evaluated without ambiguity. We thus have the finite-extension strain energy release rates for the three fracture modes as

$$\begin{Bmatrix} G_{II} \\ G_I \\ G_{III} \end{Bmatrix} = \frac{1}{2\Delta a}\int_0^{\Delta a} \begin{Bmatrix} \sigma_{xz}(r,0)\Delta u(\Delta a - r, \pi) \\ \sigma_{zz}(r,0)\Delta w(\Delta a - r, \pi) \\ \sigma_{yz}(r,0)\Delta v(\Delta a - r, \pi) \end{Bmatrix} \mathrm{d}r \tag{15}$$

where σ_{xz}, σ_{yz}, and σ_{zz} are the stresses and Δu, Δv, and Δw are the relative crack surface displacements in the x, y, and z directions, respectively. The stress intensity factors K_I, K_{II}, and K_{III} associated with an arbitrarily chosen length $\hat{l}$ originally defined by Wu[17] can be written as[20]

$$\begin{Bmatrix} K_{II} \\ K_I \\ K_{III} \end{Bmatrix} = \lim_{r\to 0}\sqrt{2\pi r}\,\Lambda\left\langle\!\!\left\langle \left(\frac{r}{\hat{l}}\right)^{-i\varepsilon_\alpha} \right\rangle\!\!\right\rangle \Lambda^{-1} \begin{Bmatrix} \sigma_{xz} \\ \sigma_{zz} \\ \sigma_{yz} \end{Bmatrix} \tag{16}$$

where $\langle\!\langle \cdots \rangle\!\rangle$ stands for a 3×3 diagonal matrix, Λ is the complex eigenvector matrix associated with the eigenvalue problem in Stroh formalism,[20] and ε_α ($\alpha = 1, 2, 3$) are bimaterial indexes that possess the form of $\varepsilon_1 = \varepsilon$, $\varepsilon_2 = -\varepsilon$, and $\varepsilon_3 = 0$ for interfacial cracks between two orthotropic media. The generalized Dundurs' parameter β is related to ε by $\varepsilon = (1/2\pi)\,\ln[(1+\beta)/(1-\beta)]$.

It follows from Eq. (16) that the singular crack-tip stress field is given by

$$\begin{Bmatrix} \sigma_{xz} \\ \sigma_{zz} \\ \sigma_{yz} \end{Bmatrix} = \frac{1}{\sqrt{2\pi r}}\Lambda\left\langle\!\!\left\langle \left(\frac{r}{\hat{l}}\right)^{i\varepsilon_\alpha} \right\rangle\!\!\right\rangle \Lambda^{-1} \begin{Bmatrix} K_{II} \\ K_I \\ K_{III} \end{Bmatrix} \tag{17}$$

and the relative crack surface displacements are[20]

$$\begin{Bmatrix} \Delta u \\ \Delta w \\ \Delta v \end{Bmatrix} = \sqrt{\frac{2r}{\pi}}\,\bar{\Lambda}^{-T}\left\langle\!\!\left\langle \frac{(r/\hat{l})^{i\varepsilon_\alpha}}{(1 + 2i\varepsilon_\alpha)\cosh\pi\varepsilon_\alpha} \right\rangle\!\!\right\rangle \Lambda^{-1} \begin{Bmatrix} K_{II} \\ K_I \\ K_{III} \end{Bmatrix} \tag{18}$$

with $\bar{\Lambda}$ indicating the conjugate of Λ. From Eq. (17) one can see that the near-tip stress field is oscillatory except for cases where $\varepsilon = 0$ or $\beta = 0$. For $\beta = 0$ the near-tip stress field assumes the regular inverse square root singularity.

Substitution of Eqs. (17) and (18) into Eq. (15) gives

$$G = \lim_{\Delta a\to 0}(G_1 + G_{II} + G_{III})$$

$$= \frac{1}{4}\left[\frac{d_{22}}{\cosh^2\pi\varepsilon}K_I^2 + \left(d_{11} - \frac{w_{21}^2}{d_{22}}\right)K_{II}^2 + \left(d_{33} - \frac{w_{32}^2}{d_{22}}\right)K_{III}^2 + 2\left(d_{13} + \frac{w_{21}w_{32}}{d_{22}}\right)K_{II}K_{III}\right] \tag{19}$$

where d_{11}, d_{22}, d_{33}, d_{13}, w_{21}, and w_{32} are elements of a bimaterial matrix.[20] Equation (19) clearly shows that the total strain energy release rate is well defined and related to the stress intensity factors.

For interfacial cracks in orthotropic media with their principal material axes aligned with the reference coordinate axes, Eq. (19) can be simplified to

$$G = (1/4\cosh^2\pi\varepsilon)\left(d_{22}K_I^2 + d_{11}K_{II}^2\right) + d_{33}K_{III}^2 \tag{20}$$

For interfacial cracks in isotropic media, Eq. (20) further reduces to

$$G = D\left(K_I^2 + K_{II}^2\right) + \tfrac{1}{4} d_{33} K_{III}^2 \tag{21}$$

where the bimaterial-dependent constant D can be found in Ref. 24 as $D = \frac{1}{16}[(\kappa_1 + 1)/\mu_1 + (\kappa_2 + 1)/\mu_2]$, with subscripts 1 and 2 designating the two different materials bounding the crack.

For two-dimensional interfacial crack problems of orthotropic media with their principal material axes aligned with the reference coordinate axes, Davidson et al.[28] defined the strain energy release rates and stress intensity factors for the two individual fracture modes as

$$\bar{G}_I = \frac{1}{2}\left[-N_c\sqrt{c_{11}}\sin\hat{\Omega} - M_c\sqrt{c_{22}}\cos(\hat{\Omega} + \Gamma)\right]^2 = \frac{H_{11}}{4\cosh^2 \pi\varepsilon}\bar{K}_I^2 \tag{22a}$$

$$\bar{G}_{II} = \frac{1}{2}\left[N_c\sqrt{c_{11}}\cos\hat{\Omega} - M_c\sqrt{c_{22}}\sin(\hat{\Omega} + \Gamma)\right]^2 = \frac{H_{11}}{4\cosh^2 \pi\varepsilon}\bar{K}_{II}^2 \tag{22b}$$

$$\bar{K}_I + i\bar{K}_{II} = \lim_{r\to 0}\sqrt{2\pi r}\left(\frac{r}{\hat{l}}\right)^{-i\varepsilon}\left(\sqrt{\frac{H_{33}}{H_{11}}}\sigma_{zz} + i\sigma_{xz}\right) \tag{22c}$$

where $\Gamma = -\sin^{-1}[c_{12}/\sqrt{(c_{11}c_{22})}]$; $\hat{\Omega} = \Omega + \varepsilon \ln(\hat{l}/l)$ in which l is a characteristic dimension and Ω a constant to be determined; and H_{11} and H_{33} are bimaterial-dependent constants. The stress intensity factors $\bar{K}_I$ and $\bar{K}_{II}$ can be related to K_I and K_{II} by the stresses σ_{xz} and σ_{zz} in Eqs. (16) and (22c).

The definitions of $\bar{G}_I$ and $\bar{G}_{II}$ yield the total strain energy release rate as

$$G = \bar{G}_I + \bar{G}_{II} = \frac{H_{11}}{4\cosh^2 \pi\varepsilon}\left(\bar{K}_I^2 + \bar{K}_{II}^2\right) \tag{23}$$

$\bar{G}_I$ and $\bar{G}_{II}$ given by Eqs. (22a) and (22b) are not the conventionally defined strain energy release rates as given by Eq. (15). They cannot be calculated using the crack closure method.

Mode Separation

Fracture mode separation can be achieved analytically by equating the total strain energy release rate obtained from the crack-tip element model with that in the G-K relation from the three-dimensional near-tip solution.

From linearity consideration, the relations between the stress intensity factors and the crack-tip generalized forces can be written as

$$\begin{Bmatrix} K_I \\ K_{II} \\ k_{III} \end{Bmatrix} = \begin{bmatrix} e_1 & e_2 & e_3 \\ e_4 & e_5 & e_6 \\ e_7 & e_8 & e_9 \end{bmatrix} \begin{Bmatrix} N_c \\ M_c \\ S_c \end{Bmatrix} \tag{24}$$

where $e_1, \ldots, e_9$ are constants to be determined. Substituting Eq. (24) into Eq. (19) and comparing the coefficients of the resulting expression of G with Eq. (13) yield six equations for determining e_i ($i = 1, 2, \ldots, 9$). Thus, three additional conditions are needed to fully determine the nine coefficients, which can be done by implementing two supplementary finite element analyses with two special load combinations, respectively. In these two finite element analyses the finite crack extension strain energy release rates are obtained using the well-known modified virtual crack closure technique, and the stress intensity factors are calculated using the displacement ratio method,[26] which employs the relationship between the stress intensity factors and the ratios of the relative crack surface displacements as given by Eq. (18).

One of the two special load combinations is chosen such that $N_c = S_c = 0$. Using this load condition, we obtain from Eq. (24)

$$e_5 = (K_{II}/K_I)e_2 \tag{25}$$

$$e_8 = (K_{III}/K_I)e_2 \tag{26}$$

in which K_I, K_{II}, and K_{III} are evaluated with this loading. The second special loading case is given by $M_c = S_c = 0$, which leads to

$$e_7 = (K_{III}/K_{II})e_4 \tag{27}$$

With these three supplementary equations, Eqs. (25–27), the nine coefficients e_i ($i = 1, 2, \ldots, 9$) can be determined.

Once the coefficients e_i ($i = 1, \ldots, 9$) are determined, the plate CTE model is completely established, and the model can be used to further calculate the stress intensity factors with Eq. (24) for the same delamination crack and geometry under other load combinations. The local loading for the CTE can first be determined from an overall plate analysis; the crack-tip generalized forces are subsequently calculated from Eq. (2).

In the preceding analysis procedure we need to carry out only one or two finite element analyses for specially selected loads to establish the plate CTE. The fracture modes for general loading can easily be separated analytically based on the plate solution.[32] For this reason the present CTE approach for separating fracture modes is computationally efficient.

Numerical Examples and Discussion

The following three examples are given to validate the preceding procedure for fracture mode separations. All of the numerical examples considered have a straight delamination as shown in Fig. 1. Uniform loads are applied along the straight edges. The local loads on the plate CTE are thus readily obtained because they are statically determinate. Note that in the first two example problems the stress intensity factors follow the definitions given by Eq. (22c), whereas in example 3 they are defined by Eq. (16).

The finite element analyses (FEA) were carried out using the commercially available FEA code ABAQUS. The eight-node isoparametric element and 20-node brick element were adopted for two-dimensional and three-dimensional analyses, respectively.

Example 1: Delamination in Isotropic Bimaterials

A double cantilever beam of two isotropic materials with unequal thicknesses was considered (Fig. 1). Relevant data used were the following[28]: $a = b = 8(t_1 + t_2)$, $t_1 = 0.04$, $t_2 = 0.08$, $E_1 = 1$, $\nu_1 = 0.2$, $E_2 = 2.333$, and $\nu_2 = 0.467$. The material constants lead to $\varepsilon = 0.06454$. A plane stress state parallel to the x-z plane was assumed. A loading case with $N_1 = 0$, $N_2 = 0$, $M_1 = 2.0075$, and $M_2 = 7.9925$, which results in $M_c = 0$, was chosen to provide additional information for determining e_i ($i = 1, 2, 4, 5$). In addition, $\hat{l} = 2a$ and $l = t_1$ were taken in calculating the stress intensity factors. This problem was also solved by Davidson et al.[28] using the displacement method in which the near-tip crack surface displacements in conjunction with their relations with the stress intensity factors were directly employed to calculate the stress intensity factors.

Listed in Table 1 are the strain energy release rates and the fracture mode phase angle defined as $\psi = \tan^{-1}(\bar{K}_{II}/\bar{K}_I)$ for four different meshes with increasing refinements. The finite element size at the crack tip is designated as Δa. The finite-extension strain energy release rates for the two individual fracture modes vary for different meshes, whereas the total strain energy release rate is more or less mesh-independent. The present results for the total strain energy release rate and phase angle agree very well with those obtained by Davidson et al.[28] A fine mesh is required to guarantee converged stress intensity factors, and for such fine meshes the stress intensity factors practically remain unchanged.

Table 1 Strain energy release rates and phase angle from FEA for delamination in an isotropic bimaterial using different meshes

Mesh	$\Delta a/a$, %	G_I	G_{II}	G	ψ, deg
A	0.130	844	476,814	477,658	−72.35
B	0.065	1,452	474,058	475,510	−70.23
C	0.033	5,640	469,357	474,997	−70.20
D	0.016	11,681	463,346	475,027	−70.20
Davidson et al.[28]	0.008	——	——	474,936	−69.88

Table 2 Comparison of solutions obtained using the FEA and the present CTE for delamination in an isotropic bimaterial

Method	G	$\bar{K}_I$	$\bar{K}_{II}$
FEA	98,728	348.23	−150.69
CTE	98,774	348.52	−150.26

Table 3 Phase angle and mode-mixity parameter for delamination in $[90/-55/55//0]_s$ laminate subjected to $M_1 = -M_2 = 1$

Parameter	Present method, deg	Davidson et al.,[31] deg
ψ	−43.947	−35.64
Ω	9.205	17.51

From the results given by mesh D, we found

$$e_1 = -5.1707, \qquad e_2 = -367.27$$

$$e_4 = 7.6329, \qquad e_5 = 58.244$$

Using the preceding values of the coefficients e_i ($i = 1, 2, 4, 5$), the stress intensity factors for a different load combination $N_1 = 0$, $N_2 = 0$, $M_1 = 1$, and $M_2 = -1$ were then calculated. Comparisons are made in Table 2 between the present CTE and the FEA solutions. The two results agree very well.

Example 2: Delamination in Orthotropic Bimaterials

Consider a $[90/-55/55//0]_s$ laminate (where // indicates the location of delamination) of infinite extent in the y direction. The straight edges are subjected to uniform normal extensional force and bending moment, but the in-plane shear force is absent. The principal material constants for the original lamina are $E_1 = 134.4$ GPa, $E_2 = E_3 = 10.2$ GPa, $\nu_{12} = \nu_{13} = 0.3$, $\nu_{23} = 0.49$, $G_{12} = G_{13} = 5.52$ GPa, and $G_{23} = 3.43$ GPa. Davidson et al.[31] solved the problem by smearing the $[\mp 55]$ sublaminate into an equivalent orthotropic layer and assuming a plane strain state parallel to the x–z plane. (The present layup $[90/-55/55//0]_s$ corresponds to the layup $[0/35/-35//90]_s$ used in Ref. 31.) After smearing, the equivalent elastic constants for the $[\mp 55]$ sublaminate are[30] $E_1 = 35.33$ GPa, $E_2 = 13.2$ GPa, $E_3 = 10.2$ GPa, $\nu_{12} = 1.137$, $\nu_{13} = -0.124$, $\nu_{23} = 0.274$, $G_{12} = 31.43$ GPa, $G_{13} = 4.83$ GPa, and $G_{23} = 4.12$ GPa. The ply thickness is 1.372×10^{-4} m. Both a and b (Fig. 1) were taken as eight times the total thickness of the laminate. In addition, we chose $\hat{l} = l = t_1$.

Taking the smeared material constants for the $[\mp 55]$ sublaminate, the cracked laminate was studied using the present approach. To determine the coefficients e_i, we needed to perform a two-dimensional plane strain finite element analysis for a specific loading. We chose the load combination of $M_1 = -M_2 = 1$ and $N_1 = N_2 = S_1 = S_2 = 0$, which results in $N_c = 0$, $M_c = -1$, and $S_c = 0$ for the FEA. A mesh with $\Delta a/a = 0.1\%$ was used. The displacement ratio method[26] was used to obtain the ratio of stress intensity factors. The phase angle ψ and mode-mixity parameter Ω are presented in Table 3. The results given by Ref. 31 are also listed. Note that the phase angle −35.64 deg was extracted from the mode-mixity parameter 17.51 deg provided in Ref. 31. The observation is made that the results given by Davidson et al.[31] are rather different from the present results.

Using $\Omega = 9.205$ deg, we obtained

$$e_1 = 6.83, \qquad e_2 = -1.30 \times 10^5$$

$$e_4 = 78.7, \qquad e_5 = 3.20 \times 10^5$$

Further calculations using the plate CTE for the same cracked laminate were conducted for other load combinations using the preceding values of Ω and e_i ($i = 1, 2, 4, 5$). Results are presented in Table 4 for the following four cases:

Table 4 Comparison of phase angle for delamination in $[90/-55/55//0]_s$ laminate subjected to various loads

Load case	ψ, deg		
	FEA	CTE	Davidson et al.[31]
1	−54.520	−54.249	−45.80
2	−10.327	−9.605	−1.19
3	32.827	36.100	44.06
4	78.140	81.030	89.07

Table 5 Total strain energy release rate ($\times 10^7$ N/m) for delamination in $[\theta_1//\theta_2]$ laminates

$[\theta_1//\theta_2]$	[0//0]	[15//0]	[45//0]	[75//0]
CTE	9.950	13.19	38.32	107.0
FEA	9.954	13.20	38.36	107.4

1) $N_c = -5144$ N/m, $M_c = -2.758$ Nm/m, and $S_c = 0$.
2) $N_c = 16{,}186$ N/m, $M_c = -5.827$ Nm/m, and $S_c = 0$.
3) $N_c = 28{,}394$ N/m, $M_c = -5.516$ Nm/m, and $S_c = 0$.
4) $N_c = 23{,}961$ N/m, $M_c = -1.957$ Nm/m, and $S_c = 0$.

For each loading case a two-dimensional plane strain FEA was also performed to obtain the phase angle ψ. The present CTE analyses yield good results for the fracture mode phase angle when compared with the FEAs. Clearly, the corresponding phase angle and thus the stress intensity factors given by Davidson et al.[31] are somewhat different from the present results. The difference in phase angle for each loading case from the present CTE analysis and that by Davidson et al.[31] is about 8 deg. Both Tables 3 and 4 indicate that the direct displacement method employed by Davidson et al.[31] is not so accurate for calculating the stress intensity factors for delamination cracks in platelike composite structures. To accurately extract the stress intensity factors using the direct displacement method as was adopted in Ref. 31, exceedingly fine finite element meshes around the crack tip must be used.

Example 3: Delamination in Multidirectional Composite Laminates

Consider a multidirectional composite laminate in pseudo-three-dimensional deformation (i.e., generalized plane strain) for which the stresses and strains are independent of the y axis. In reality, the assumption of pseudo-three-dimensional deformation is a good approximation when the laminate is relatively long in the y direction and the loading is independent of y. For such a delamination problem in multidirectional composite laminates, all three fracture modes may exist. In the FEA the pseudo-three-dimensional condition can be realized by modeling the laminate with one layer of three-dimensional brick elements in the y direction and tying all of the corresponding nodes on the front and back faces of the laminate. The ply properties used were $E_1 = 134.4$ GPa, $E_2 = E_3 = 10.2$ GPa, $\nu_{12} = \nu_{13} = 0.3$, $\nu_{23} = 0.49$, $G_{12} = G_{13} = 5.52$ GPa, and $G_{23} = 3.43$ GPa. The length scale $\hat{l} = 2a$ was adopted in calculating the stress intensity factors.

Uniform Edge Loading

First, consider two-ply $[\theta_1 // \theta_2]$ laminates with edge delamination similar to that shown in Fig. 1. The geometry of the delaminated laminate is the same as that in example 1. The total energy release rate can be calculated using the present CTE and laminated-plate theory. Table 5 shows the total strain energy release rates for various cracked angle ply laminates subjected to the load combination of $N_1 = 50$ N/m, $N_2 = -80$ N/m, $M_1 = 1$ Nm/m, $M_2 = -2$ Nm/m, and $S_1 = S_2 = 0$. For comparison pseudo-three-dimensional FEAs for the total strain energy release rate were also performed. The CTE model can generate very accurate values of the total strain energy release rate for delamination cracks in general composite laminates.

For mode separations the coefficients e_i need to be determined. The following two special loading cases were chosen for the supplementary FEAs:

1) $M_1 = 1$ Nm/m, $M_2 = -1$ Nm/m, $N_1 = N_2 = 0$, and $S_1 = S_2 = 0$, which leads to $N_c = S_c = 0$.

Table 6 Ratios of stress intensity factors from FEA for delamination in [45//0] laminate for loading case 1 with $N_c = S_c = 0$

Node pair	K_{II}/K_I	K_{III}/K_I	K_{III}/K_{II}
1	1.1098	0.22883	0.20619
2	1.2748	0.26753	0.20987
3	1.2623	0.26792	0.21226
4	1.2547	0.26454	0.21084
5	1.2389	0.26093	0.21061

Table 7 Ratios of stress intensity factors from FEA for delamination in [45//0] laminate for loading case 2 with $M_c = S_c = 0$

Node pair	K_{II}/K_I	K_{III}/K_I	K_{III}/K_{II}
1	−10.052	−3.8371	0.38171
2	−12.228	−4.5782	0.37257
3	−14.953	−5.5067	0.36828
4	−16.277	−5.9276	0.36417
5	−17.981	−6.5361	0.36350

2) $M_1 = 1$ Nm/m, $M_2 = -1$ Nm/m, $N_1 = 56.547$ N/m, $N_2 = -423.51$ N/m, and $S_1 = S_2 = 0$, which leads to $M_c = S_c = 0$.

Tables 6 and 7 show the ratios of stress intensity factors for the [45//0] laminate computed using the displacement ratio method at the five pairs of nodes closest to the crack tip for load combinations 1 and 2, respectively. Although theoretically the solutions at the first pair of nodes are the best approximation to the crack-tip displacements, they are not accurate because of the singular nature of the near-tip stress field. The displacement ratios at the second, third, or fourth pair of nodes were found to yield more accurate solutions. These two tables show that the ratios K_{II}/K_I and K_{III}/K_I for case 1 and K_{III}/K_{II} for case 2 do not vary significantly and thus were chosen for determining e_i ($i = 1, 2, \ldots, 9$). Taking these three ratios of stress intensity factors at the third pair of nodes, we obtained

$$e_1 = 0.26872, \quad e_2 = -130.93, \quad e_3 = 0.67218$$

$$e_4 = -6.8091, \quad e_5 = -164.28, \quad e_6 = -0.92568$$

$$e_7 = -2.4797, \quad e_8 = -34.637, \quad e_9 = -4.9811$$

Further calculations for mode mixities were carried out for the following loading cases:

1) $M_1 = 1$ Nm/m, $M_2 = 1$ Nm/m, $N_1 = N_2 = 0$, and $S_1 = S_2 = 0$.

2) $N_1 = -50$ Nm/m, $N_2 = 80$ Nm/m, $M_1 = M_2 = 0$, and $S_1 = S_2 = 0$.

3) $N_1 = 50$ Nm/m, $N_2 = -80$ Nm/m, $M_1 = 1$ Nm/m, $M_2 = -2$ Nm/m, and $S_1 = S_2 = 0$.

4) $N_1 = 50$ Nm/m, $N_2 = -80$ Nm/m, $M_1 = 2$ Nm/m, $M_2 = -1$ Nm/m, and $S_1 = S_2 = 0$.

For comparison, pseudo-three-dimensional FEAs using solid brick elements were also conducted. The CTE predicted stress intensity factors and their FEA counterparts are compared in Table 8. Even if the laminate is subjected to a single-mode loading, as in cases 1 and 2, all three fracture modes are present because of the asymmetry in material properties and laminate geometry. The crack-tip generalized shear force S_c is nonzero in either loading case. In general, the CTE and FEA results agree very well. The discrepancy increases as the load combination for the laminate changes from a single-mode loading to a mixed-mode loading. In the case where there is a dominant fracture mode, the CTE predictions for the other two nondominant modes are not as accurate in some loading cases.

Uniform Stretching

Consider the edge delamination problem of a $[90/-55/55//0]_s$ laminate subjected to a uniform axial strain ε_{yy}. The geometry was taken to be the same as that of example 2. Three models were used for analysis: 1) the laminate was forced to deform in generalized plane strain condition; i.e., a plane cross section remains plane during loading. In this case the angle ply group $[\mp 55]$ was smeared into an equivalent orthotropic layer; 2) in addition to the assumptions made in model 1, one of the Poisson's ratios was changed from −0.124 in model 1 to 0.5632 so that $\beta = 0$; and 3) the laminate deformed in the pseudo-three-dimensional condition. The identities of the individual plies are kept in the pseudo-three-dimensional analysis. The results of this model should be considered as "exact."

Table 8 Comparison of stress intensity factors from CTE and FEA for delamination in [45//0] laminate subjected to various loads

Load case	K_I, Pa $\sqrt{\text{m}}$		K_{II}		K_{III}	
	CTE	FEA	CTE	FEA	CTE	FEA
1	95.0	95.9	191	190	33.9	35.4
2	94.0	94.7	−142	−147	−90.7	−85.9
3	54.9	38.6	293	298	126	126
4	150	140	484	499	160	169

Table 9 Comparison of strain energy release rates and stress intensity factors from FEA for edge delamination in $[90/-55/55//0]_s$ laminate subjected to $\varepsilon_{yy} = 0.254\%$

Model	G, N/m	K_I, Pa $\sqrt{\text{m}}$	K_{II}	K_{III}
1	19.026	2.346	5.370	0
2	19.011	3.183	5.126	0
3	19.878	1.661	6.242	−0.468

Using the finite element method, the strain energy release rates and stress intensity factors for the preceding three models with $\varepsilon_{yy} = 0.254\%$ were calculated using a near-tip mesh of $\Delta a/a = 0.1\%$. The results are listed in Table 9. The total strain energy release rate has an error of 4.6% when model 1 is used. Under such a generalized plane strain condition, the stress intensity factors are rather different from those obtained using the pseudo-three-dimensional analysis. The artificial adjustment of Poisson's ratio in model 2 to render $\beta = 0$ can lead to even greater errors in the stress intensity factors.

Conclusions

An approach combining a plate CTE model and a fracture mode separation technique was developed to calculate stress intensity factors and mode mixities for delamination cracks in platelike laminated composite structures. The plate CTE in conjunction with the finite element method was used to separate fracture modes in cracked platelike structures. The CTE method was shown to be efficient in analyzing delamination cracks in composite laminates. Examples were provided to illustrate the mode separation procedure. The following conclusions have been obtained:

1) Generally, the present CTE method can be used to calculate accurately the stress intensity factors for delamination cracks in general composite laminates. However, in cases where there exists a dominant fracture mode, significant errors may occur in the smallest stress intensity factor predicted by the present method.

2) Smearing $[\pm\theta]$ angle plies and replacing them with an equivalent homogeneous orthotropic layer could cause some inaccuracy in calculating stress intensity factors.

3) For general composite laminates the approach based on the assumption $\beta = 0$ to remove the oscillatory behavior of stresses at the crack tip may give rise to appreciable errors.

Acknowledgment

This work was supported by a NASA Langley Research Center Grant (NAG-1-1323) to Purdue University.

References

[1] Williams, M. L., "The Stresses Around a Fault or Crack in Dissimilar Media," *Bulletin of the Seismological Society of America*, Vol. 49, 1959, pp. 199–204.

[2] England, A. H., "A Crack Between Dissimilar Media," *Journal of Applied Mechanics*, Vol. 32, June 1965, pp. 400–402.

[3] Rice, J. R., and Sih, G. C., "Plane Problems of Cracks in Dissimilar Media," *Journal of Applied Mechanics*, Vol. 32, June 1965, pp. 418–423.

[4]Malysev, B. M., and Salganik, R. L., "The Strength of Adhesive Joints Using the Theory of Cracks," *International Journal of Fracture*, Vol. 1, 1965, pp. 114–127.

[5]Sun, C. T., and Jih, C. J., "On Strain Energy Release Rate for Interfacial Cracks in Bimaterial Media," *Engineering Fracture Mechanics*, Vol. 28, No. 1, 1987, pp. 13–20.

[6]Hutchinson, J. W., Mear, M., and Rice, J. R., "Crack Paralleling an Interface Between Dissimilar Materials," *Journal of Applied Mechanics*, Vol. 54, Dec. 1987, pp. 828–832.

[7]Rice, J. R., "Elastic Fracture Mechanics Concepts for Interfacial Cracks," *Journal of Applied Mechanics*, Vol. 55, March 1988, pp. 98–103.

[8]Gotoh, M., "Some Problems of Bonded Anisotropic Plates with Crack Along the Bond," *International Journal of Fracture*, Vol. 3, 1967, pp. 253–265.

[9]Clements, D. L., "A Crack Between Dissimilar Anisotropic Media," *International Journal of Engineering Science*, Vol. 9, 1971, pp. 257–265.

[10]Willis, J. R., "Fracture Mechanics of Interfacial Cracks," *Journal of the Mechanics and Physics of Solids*, Vol. 19, 1971, pp. 353–368.

[11]Wang, S. S., and Choi, I., "The Interface Crack Between Dissimilar Anisotropic Materials," *Journal of Applied Mechanics*, Vol. 50, March 1983, pp. 169–178.

[12]Wang, S. S., and Choi, I., "The Interface Crack Between Dissimilar Anisotropic Composites Under Mixed-Mode Loading," *Journal of Applied Mechanics*, Vol. 50, March 1983, pp. 179–183.

[13]Ting, T. C. T., "Explicit Solution and Invariance of the Singularities at an Interface Crack in Anisotropic Composites," *International Journal of Solids and Structures*, Vol. 22, No. 9, 1986, pp. 965–983.

[14]Bassani, J. L., and Qu, J., "Finite Crack on Bimaterial and Bicrystal Interfaces," *Journal of the Mechanics and Physics of Solids*, Vol. 37, No. 4, 1989, pp. 435–453.

[15]Sun, C. T., and Manoharan, M. G., "Strain Energy Release Rates of an Interfacial Crack Between Two Orthotropic Solids," *Journal of Composite Materials*, Vol. 23, No. 5, 1989, pp. 460–478.

[16]Manoharan, M. G., and Sun, C. T., "Strain Energy Release Rates of an Interfacial Crack Between Two Anisotropic Solids Under Uniform Axial Strain," *Composites Science and Technology*, Vol. 39, No. 2, 1990, pp. 99–116.

[17]Wu, K. C., "Stress Intensity Factor and Energy Release Rate for Interfacial Cracks Between Dissimilar Anisotropic Materials," *Journal of Applied Mechanics*, Vol. 57, Dec. 1990, pp. 882–886.

[18]Suo, Z., "Singularities, Interfaces and Cracks in Dissimilar Anisotropic Media," *Proceedings of the Royal Society of London*, Vol. A427, 1990, pp. 331–358.

[19]Gao, H., Abbudi, M., and Barnett, D. M., "Interfacial Crack-Tip Field in Anisotropic Elastic Solids," *Journal of the Mechanics and Physics of Solids*, Vol. 40, No. 2, 1992, pp. 393–416.

[20]Hwu, C., "Fracture Parameters for the Orthotropic Bimaterial Interface Cracks," *Engineering Fracture Mechanics*, Vol. 45, No. 1, 1993, pp. 89–97.

[21]Hwu, C., "Explicit Solutions for Collinear Interface Crack Problems," *International Journal of Solids and Structures*, Vol. 3, No. 3, 1993, pp. 301–312.

[22]Deng, X., "General Crack Tip Fields for Stationary and Steadily Growing Interface Cracks in Anisotropic Bimaterials," *Journal of Applied Mechanics*, Vol. 60, 1993, pp. 183–189.

[23]Matos, P. P. L., McMeeking, R. M., Charalambides, P. G., and Dory, M. D., "A Method for Calculating Stress Intensities in Bimaterial Fracture," *International Journal of Fracture*, Vol. 40, 1989, pp. 235–254.

[24]Sun, C. T., and Qian, W., "The Use of Finite Extension Strain Energy Release Rates in Fracture of Interface Cracks," *International Journal of Solids and Structures*, Vol. 34, No. 20, 1997, pp. 2595–2609.

[25]Qian, W., and Sun, C. T., "Methods for Calculating Stress Intensity Factors for Interfacial Cracks Between Two Orthotropic Solids," *International Journal of Solids and Structures*, Vol. 35, No. 25, 1998, pp. 3317–3330.

[26]Qian, W., and Sun, C. T., "Calculation of Stress Intensity Factors for Interlaminar Cracks in Composite Laminates," *Composites Science and Technology*, Vol. 57, No. 6, 1997, pp. 637–650.

[27]Schapery, R. A., and Davidson, B. D., "Prediction of Energy Release Rate for Mixed-Mode Delamination Using Classical Plate Theory," *Applied Mechanics Review*, Vol. 43, No. 5, 1990, pp. S281–S287.

[28]Davidson, B. D., Hu, H., and Schapery, R. A., "An Analytical Crack-Tip Element for Layered Elastic Structures," *Journal of Applied Mechanics*, Vol. 62, June 1995, pp. 294–305.

[29]Davidson, B. D., "Prediction of Delamination Growth in Laminated Structures," *Failure Mechanics in Advanced Polymeric Composites*, edited by G. A. Kardomateas and Y. D. S. Rajapakse, Applied Mechanics Div., AMD Vol. 196, American Society of Mechanical Engineers, New York, 1994, pp. 43–65.

[30]Davidson, B. D., "Prediction of Energy Release Rate for Edge Delamination Using a Crack Tip Element Approach," *Composite Materials: Fatigue and Fracture*, Vol. 5, STP 1230, edited by R. H. Martin, American Society for Testing and Materials, Philadelphia, 1995, pp. 155–175.

[31]Davidson, B. D., Hu, H., and Yan, H., "An Efficient Procedure for Determining Mixed-Mode Energy Release Rates in Practical Problems of Delamination," *Finite Elements in Analysis and Design*, Vol. 23, 1996, pp. 193–210.

[32]Jones, R. M., *Mechanics of Composite Materials*, McGraw–Hill, New York, 1975.

G. A. Kardomateas
Associate Editor